Frontiers of Physics
https://doi.org/10.1007/s11467-020-0999-8
Front. Phys.
16(1), 13503 (2021)

RESEARCH ARTICLE

Theoretical investigation of $CoTa_2O_6$/graphene heterojunctions for oxygen evolution reaction

Qinye Li[1,2], **Siyao Qiu**[3,†], **Baohua Jia**[1,2,‡]

[1] *Centre for Translational Atomaterials, Faculty of Science, Engineering and Technology, Swinburne University of Technology, Hawthorn, Victoria 3122, Australia*
[2] *The Australian Research Council (ARC) Industrial Transformation Training Centre in Surface Engineering for Advanced Materials (SEAM), Swinburne University of Technology, Hawthorn, Victoria 3122, Australia*
[3] *College of Chemical Engineering and Energy Technology, Dongguan University of Technology, Dongguan 523808, China*
Corresponding authors. E-mail: [†] *qsy333666@163.com,* [‡] *bjia@swin.edu.au*
Received August 22, 2020; accepted September 8, 2020

Water electrolysis is to split water into hydrogen and oxygen using electricity as the driving force. To obtain low-cost hydrogen in a large scale, it is critical to develop electrocatalysts based on earth abundant elements with a high efficiency. This computational work started with Cobalt on $CoTa_2O_6$ surface as the active site, $CoTa_2O_6$/Graphene heterojunctions have been explored as potential oxygen evolution reaction (OER) catalysts through density functional theory (DFT). We demonstrated that the electron transfer (δ) from $CoTa_2O_6$ to graphene substrate can be utilized to boost the reactivity of Co-site, leading to an OER overpotential as low as 0.30 V when N-doped graphene is employed. Our findings offer novel design of heterojunctions as high performance OER catalysts.

Keywords $CoTa_2O_6$, OER, charge transfer, DFT, heterojunctions

1 Introduction

Water electrolysis has been identified as a promising approach to produce hydrogen from water [1–3]. However, the multistep oxygen evolution reaction (OER: $4OH^- \rightarrow 2H_2O + 4e^- + O_2$, $E = 1.23$ V versus Reversible Hydrogen Electrode, RHE) results in sluggish kinetics, which significantly limits its commercialization [2]. Currently, IrO_2 and RuO_2 have been widely recognized as the benchmark catalysts for OER. But their high costs restrict the industry large-scale applications [4–6]. Therefore, extensive efforts have been made to develop non-noble metal-based catalysts [7–12].

To develop low-cost alternative to IrO_2 and RuO_2, a typical approach is to design OER catalysts with the use of earth abundant elements. Among various candidates, Cobalt (Co) has been widely identified as a promising element and widely explored, such as CoOOH-pristine [14], $Ag@Co(OH)_2$ [15], Co_3O_4 [16, 17], and highly dispersed Co embedded metal-organic-framework [18] and layered double hydroxides (LDH) [19]. These successes vividly demonstrated that Co–O bonding network offers high performance for OER, but the catalysis performance is sensitive to the local bonding environment.

A typical example is that the performances of Co_3O_4 facets, due to coordination difference, are remarkably different, from OER overpotential $\eta = 0.79$ V for (111) while $\eta = 0.29$ V for (110). Researchers also found that alloy elements, like V and Fe, can significantly improve OER performance when doped [17–20]. These researches not only advanced our knowledge on the reaction mechanisms, but also pointed out that the electronic states of Co-sites play the key role, which could be employed for rational design of OER catalysts.

In this work, we envisaged the design of novel Co-based OER catalysts through DFT calculations, proposing $CoTa_2O_6$/graphene heterojunctions as concept catalysts. Our hypothesis is that Co–O terminated $CoTa_2O_6$ may offer high-coverage Co-sites for OER when a graphene substrate has been employed to tune its electronic structures. As demonstrated below, the performance of pristine $CoTa_2O_6$ is not outstanding ($\eta = 0.82$ V), but when it hybrids with N-doped graphene to form heterojunctions, the overpotential is reduced to 0.30 V, which is even better than Pt (111) [21] ($\eta = 0.43$ V) and RuO_2 edges [22] ($\eta = 0.43$ V). It demonstrates that catalysts-substrate heterojunctions can be viewed as a concept structure for the rational design of catalysts for various reactions.

*Special Topic: Heterojunction and Its Applications (Ed. Chenghua Sun). This article can also be found at http://journal.hep.com.cn/fop/EN/10.1007/s11467-020-0999-8.

2 Computational methods

All calculations were carried out under the scheme of spin-polarized DFT using CASTEP [23, 24]. Specifically, the Perdew–Burke–Ernzerhof (PBE) exchange-correlation functional [25] within the generalized gradient approximation was employed to describe the exchange-correlation energy. The projector-augmented-wave [26] method was adopted for the pseudopotentials. Based on our tests, the energy cutoff for the plane wave basis expansion was set to 450 eV. During geometry optimizations, the force on each atom was set as 0.03 eV/Å for convergence criterion, together with total energy converged to 10^{-4} eV. Tighter convergence criterion can only bring very small changes (<0.06 eV) for reaction energy based on our tests. For the fabrication of $CoTa_2O_6$/graphene junction, slab model was constructed with a vacuum layer of 15 Å in the z direction to avoid the interaction between layers. The sampling in the Brillouin zone was set with 1×1×1 by the Monkhorst-Pack method due to the large size of the supercells [27]. The van der Waals interaction has been corrected based on the DFT-D3 scheme [28].

3 Results and discussion

3.1 Fabrication of $CoTa_2O_6$/graphene heterojunctions

Our target is to search for high performance Co-based catalysts, following which computational study starts from Co-rich phases. Given Co–O bonding needs to be carefully tuned to suit OER multiple steps, the second metal has also been considered at the beginning. Herein, we choose $CoTa_2O_6$ crystal, which is composed of earth-abundant Co/Ta metals and has been synthesized readily in the lab for decades [29, 30]. Its unit cell has been shown in Fig. 1(a), which is a typical trirutile type, with a space group P42/mnm, a = 4.7358 Å and c = 9.1708 Å as determined by neutron diffraction at room temperature [31]. Generally, such trirutile crystal can be written as a general formula TMX_2O_6, in which TM stands for divalent 3d transition metal cation TM^{2+}, and X for pentavalent transition metal cation [32]. Therefore, $CoTa_2O_6$ crystal presents Co^{2+} cations in square planar layers, which are separated by two neighbouring edge-connected TaO_6 octahedra. As a result, there are two metal–oxygen terminations when (001) surfaces are generated, namely Co–O and Ta–O. Given Co has been widely reported as active elements for OER, Co–O terminated surface has been employed as active surfaces for OER studies. While for the fabrication of heterojunctions, both Co–O and Ta–O terminations can hybrid with the substrate (typically carbon materials in electrochemical reactions); as a result, two possible terminations, labelled as M1 and M2, can be presented at the catalyst-substrate interface, as shown in Fig. 1(b).

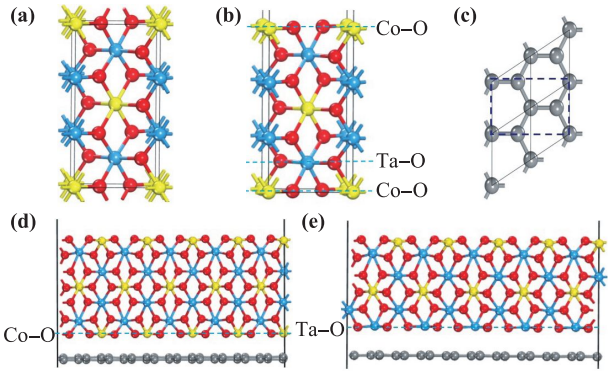

Fig. 1 Fabrication of $CoTa_2O_6$/graphene heterojunctions. **(a)** Bulk $CoTa_2O_6$; **(b)** (001) slab for $CoTa_2O_6$ showing potential Co–O (M1) and Ta–O (M2) terminations; **(c)** graphene cell (hexagon and tetragonal lattices are indicated by grey and blue lines); **(d)** M1/Graphene junction and **(e)** M2/Graphene junction. Co, Ta, O and C are shown as yellow, blue, red, and grey spheres.

To further build heterojunctions, carbon substrate has been simulated by graphene monolayer based on two considerations: (i) the interaction between graphene layers (substrate) is dominated by weak van der Waals interaction, which does not bring significant effect on the chemical bonding on catalysts surfaces; and (ii) $CoTa_2O_6$/graphene junction is already huge and it is not affordable to further extend the thickness of graphene substrate for DFT calculations. It is well known that the unit cell of graphene is hexagon, which needs to be converted to tetragonal unit before mixing with the (001) slab of $CoTa_2O_6$, as shown in Fig. 1(c). Based on the cells shown above, $CoTa_2O_6$/graphene heterojunctions can be fabricated. With a balance between the needs to minimize the computational cost and the crystal mismatch at the interface, the (5×2) supercell has been taken for $CoTa_2O_6$ (001) to hybrid with graphene supercell of (5×4) supercell. The lattice for such heterojunctions is set as the geometric mean, based on which the maximum interfacial mismatch can be reduced to 2.1%. The full-size heterojunctions will contain 290 and 260 atoms for M1 and M2, respectively, which is also the limit for our computational capacity at the DFT level. Figures 1(d) and (e) show these heterojunctions models, with Co–O and Ta–O terminations over the interface (bottom layers), labelled as M1 and M2. It is worth mentioning that both are terminated with Co–O layers on the surface layer, under which four-coordinated Co (Co_{4c}) has been considered as the active site below for catalysis investigations, as described below.

3.2 OER performance

To investigate the interfacial effect of $CoTa_2O_6$/graphene heterojunctions on OER performance, before mixing with $CoTa_2O_6$, M1 and M2 have been employed as a reference.

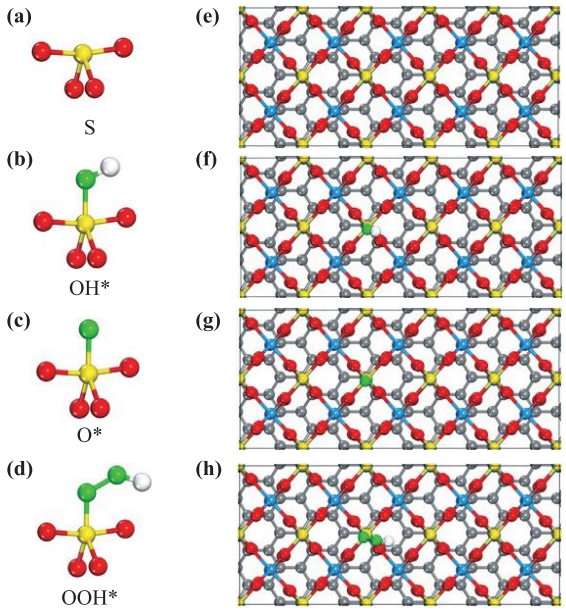

Fig. 2 Optimized geometries of intermediate states. **(a)** M1/Graphene; and **(b)** M2/Graphene. Co, Ta, O, and C in catalysts are shown as yellow, blue, red and grey spheres. O and H from water are shown as green and white spheres.

Therefore, four catalysts have been studied, including M1, M2, M1/Graphene, and M2/Graphene. All these catalysts present the same active sites (surface Co) and same coordination (Co_{4c}). The first step is to obtain the intermediate states, including clean surface (S), OH*, O*, and OOH* states based on the elementary steps involved in full OER, as well described in the literature [33–37]. After geometry optimizations of these states, it is not surprising that same intermediate states show very similar geometries in these catalysts, ensuring that the performance difference presented below essentially origins from the change of electronic structures. Therefore, we only highlighted the local bonding contained in these intermediate states, as shown in Figs. 2(a)–(d), together with intermediate states over M1/Graphene shown as an example [see Figs. 2(e)–(h)].

Now we turn to the evaluation of OER catalysis. Fig. 3 shows the free energy profiles for full OER over M1 and

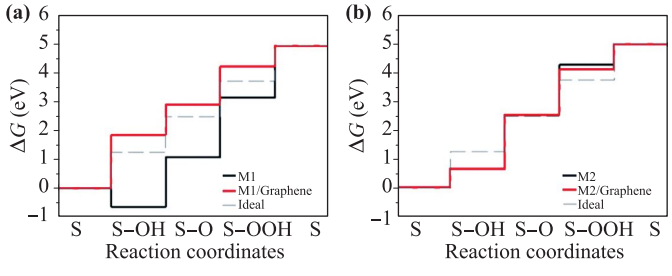

Fig. 3 Calculated OER performance. **(a)** M1/Graphene; and **(b)** M2/Graphene. S, S–OH, S–O and S–OOH indicate the intermediate states S, OH*, O*, and OOH* as described in the main text.

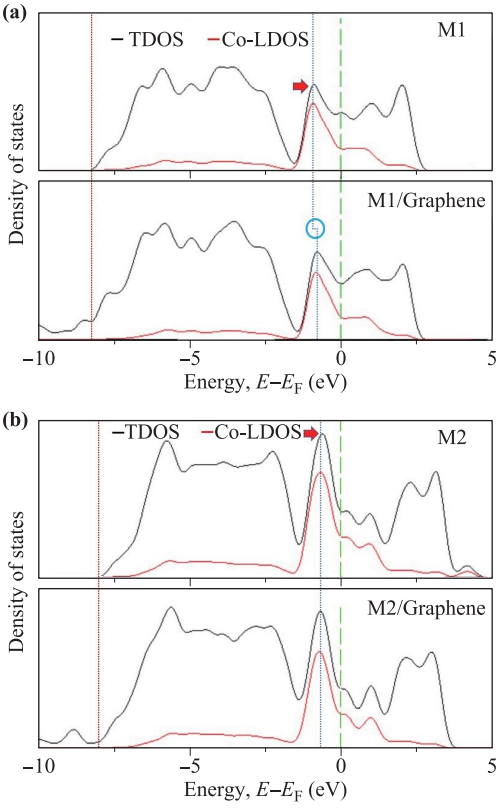

Fig. 4 Calculated DOS profiles. **(a)** M1 & M1/Graphene; and **(b)** M2 & M2/Graphene.

M2, in which the profile for ideal catalyst, as dash lines, has been employed as a reference. Theoretically, the overall free energy change ΔG for $2H_2O \rightarrow 2H_2+O_2$ is 4.92 eV per O_2; therefore, ΔG for each elementary step is 1.23 eV in the ideal case. Real catalysts always show a deviation from such ideal case, leading to an overpotential U, as determined by $U = \Delta G_{max}/(-e) - 1.23$, in which U is in unit of V, e is the natural charge for one single electron, and ΔG_{max} is the maximum ΔG derived from calculated ΔG values for four elementary steps. Following this, we obtained $\Delta G_{max} = 2.05$ eV and 1.84 eV for M1 and M2 respectively, before hybriding with graphene, indicating that surface termination can affect the catalysis performance. With the formation of heterojunctions, it is interesting that M1 has been remarkably improved, with ΔG_{max} decreasing from 2.05 eV to 1.85 eV, while M2 almost has no change ($\Delta G_{max} = 1.83$ eV). Given ΔG_{max} for original M1 and M2 shows a difference of 0.21 eV, it is worth further understanding how graphene substrate has improved M1 performance to the similar level as M2 and M2/Graphene, as explored from the electronic structures below.

3.3 Electronic modulation by a graphene substrate

Before calculating the electronic structures, it is worth noting that the active site (Co_{4c}) presents two dangling

bonds using six-coordinated Co in the bulk case as a reference. Therefore, non-bonding electrons, dominated by Co_{3d} orbitals, are resulted, which are active and should be close to the Fermi energy. Following this analysis, density of states (DOS) for M1 and M2 have been firstly calculated, including the total DOS (TDOS, black) and local DOS (LDOS, red, 20 times magnified for comparison) for surface Co as shown in Figs. 4(a) and (b), respectively, in which Fermi line is highlighted by dash green lines. Red arrows indicate the non-bonding states associated with lowly coordinated metals on the surface, being on the top of typical valence band (VB) dominated by metal-oxygen bonding in the energy window of $(-8, -2)$ in the unit of eV, with VB bottom being indicated by red dash lines. Such calculations indicate that OER reaction will be dominated by these non-bonding electronic states; therefore, our following analysis will focus on the change of this peak (indicated by red arrow).

In Fig. 4, DOS profiles for M1/Graphene and M2/Graphene are shown under M1 and M2 profiles. Accordingly, the non-bonding state in M1 shows a slight shift ($\Delta \approx 0.2$ eV, see blue circle in Fig. 4(a) towards the Fermi energy, indicating that it becomes more active. It is worth mentioning that the LDOS (red solid line) is from the reaction side, meaning that such peak shift is not due to the geometry distortion associated with interfacial mismatch and/or changes for local bonding, but essentially due to the change of Co_{4c} electronic states. Based on the calculated Mulliken charges, electrons are transferred from $CoTa_2O_6$ to the graphene substrate, mainly due to interfacial bonding. From the case of M1/Graphene, however, the interfacial interaction can also affect the electronic state on the surface, as shown by local DOS for surface Co atoms. Combining with OER performance, this interfacial effect is beneficial to improve Co_{4c} activity as demonstrated in Fig. 3(a). Interestingly, the peak shift observed in M1/Graphene has not been found in the case of M2/Graphene, as shown in Fig. 4(b), in which the positions of non-bonding states in M2 and M2/Graphene are almost the same, being around at -0.8 eV. Given the essential difference between M1 and M2 termination employed to hybrid with graphene, it appears that Co–O (M1) and Ta–O (M2) terminations have different capacity to interact with graphene substrate. Such conclusion has been supported by the calculated electron transfer $\delta = 0.86$ e and 0.22 e for M1/Graphene and M2/Graphene, respectively. Overall, it is concluded that different interfacial bonding results in the observed difference of electronic modulation by the graphene substrate, highlighting the value of rational optimization of interfacial bonding for further improvement of OER performance for such heterojunctions.

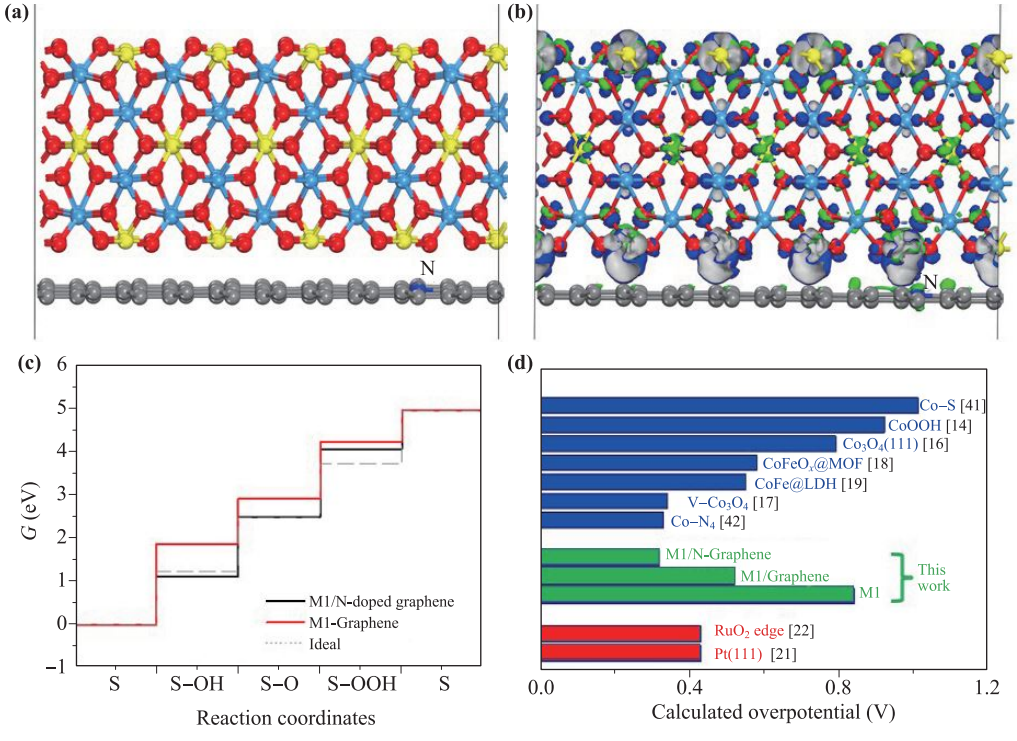

Fig. 5 N-doping effect. **(a)** $CoTa_2O_6$/N-Graphene model; **(b)** Charge density difference for the heterojunction, with green and blue isosurfaces to indicate electron accumulation and deficiency (isovalue of 0.02 e/Å^3); **(c)** Calculated free energy profiles for elementary steps; and **(d)** Overpotential comparison with literature results (black number after each catalyst is the reference number).

3.4 Strengthened electron transfer using N-doped graphene

Following the analysis above, it is worth exploring whether OER performance can be further improved when electron transfer from $CoTa_2O_6$ to the graphene substrate is strengthened. This is not difficult for lab-based practice because N-doped graphene (N-Graphene) has been readily synthesized experimentally [38]. In fact, turning electronic states has been well considered in Graphene-based junctions for catalyst design [39, 40]. Herein, we hypothesized that N-dopants, due to stronger electronegativity than carbon, can strengthen electron transfer and further tune the electronic states of Co_{4c}. To validate such hypothesis, M1/N-Graphene heterojunctions has been built (N-doping concentration, 1/80, blue sphere representing N-dopant), as shown in Fig. 5(a). After geometry optimization, it is found that electron transferred from $CoTa_2O_6$ to graphene substrate increases from 0.86 e to 1.07 e, confirming our hypothesis that N-doping can strengthen the electron transfer from $CoTa_2O_6$ to the graphene substrate.

Figure 5(b) shows the calculated charge density difference, with $\Delta\rho$=ρ($CoTa_2O_6$/N-graphene) − ρ($CoTa_2O_6$) − ρ(N-graphene), in which electron accumulation and deficiency are shown as blue and green isosurfaces. According to this result, three critical features can be summarized: (i) $CoTa_2O_6$àGraphene electron transfer can be vividly seen because graphene monolayer shows net electron accumulation, which is consistent with Mulliken charge population; (ii) lowly coordinated Co-atoms at the interface are the major channels to transfer the electrons; and (iii) transferred electrons are mainly located at N-dopants areas, confirming the role of N-dopants. Therefore, the hypothesis that electron transfer can be improved through N-doping has been well supported.

It is vital to further examine whether N-doping in the substrate can boost OER performance of surface Co_{4c}. Figure 4c shows the calculated free energy, according to which M1/N-Graphene performance is obviously better than that of M1/Graphene, with the maximum free energy change (ΔG_{max}) decreases from 1.85 eV to 1.55 eV. As a result, its profile is closer to the ideal catalysts and shows an overpotential η = 0.32 V, even lower than that achieved by Pt (111) (η=0.43 V, [21]) and RuO_2 edges (η = 0.43 V, [22]). A better comparison with literature in the past couple of years [14, 16–22, 41, 42] has been presented in Fig. 5d. Therefore, $CoTa_2O_6$/N-Graphene can be viewed as a promising low-cost OER catalyst. It is worth pointing out that the high performance does not origin from $CoTa_2O_6$ itself as shown by M1 and M2 in Fig. 3, highlighting the importance of the graphene substrate. This is quite informative because carbon substrates have been widely employed in electrocatalysis and experimental technique for the proposed N-doping has been well established. Another point worth mentioning is the high coverage of Co_{4c} active sites, making it particularly attractive with respect to low-loading single-atom catalysts. In future, Co-, Fe-, and Ni-rich compounds can be further explored to optimize the performance and reduce the cost through rational design of catalysts/substrate heterojunctions. Computer-aided optimization of the catalyst-substrate interaction demonstrated in this work can be employed as a useful guideline for such designs. In fact, a series of heterojunction catalysts using two dimensional materials as the substrate have been proposed, demonstrating that both catalyst and catalyst-substrate interface play vital roles for various applications [43–45].

4 Conclusion

In summary, $CoTa_2O_6$, as Co-based OER catalysts, has been employed to design $CoTa_2O_6$/Graphene heterojunctions. Their OER performances have been investigated under DFT scheme, focusing on the effect of surface termination and interfacial bonding on OER catalysis performance. With the same Co–O surface for OER, the reactivity with another side terminated by Ta–O (M2 case) is higher than that by Co–O termination (M1 case). After mixing with graphene to form heterojunctions, however, M1/Graphene offers similar performance with M2, due to an improvement in charge transfer. OER performance can be further improved when N-doped graphene is introduced to fabricate M1/N-Graphene heterojunction, offering an overpotential as low as 0.32 V at standard conditions. This fundamental study demonstrates the possibility to optimize the substrate and interfacial bonding to improve catalyst performance, which can be employed as a strategy for the rational design of catalysts.

Acknowledgements B. J. and Q. L. acknowledge the support through the Australia Research Council Industrial Transformation Training Centres scheme (Grant No. IC180100005). The authors acknowledge the financial support by Guangdong Innovation Research Team for Higher Education (Grant No. 2017KCXTD030) and High-level Talents Project of Dongguan University of Technology (Grant No. KCYKYQD2017017) and Engineering Research Center of None-food Biomass Efficient Pyrolysis and Utilization Technology of Guangdong Higher Education Institutes (Grant No. 2016GCZX009).

References

1. M. G. Walter, E. L. Warren, J. R. McKone, S. W. Boettcher, Q. Mi, E. A. Santori, and N. S. Lewis, Solar water splitting cells, *Chem. Rev.* 110(11), 6446 (2010)

2. H. Dau, C. Limberg, T. Reier, M. Risch, S. Roggan, and P. Strasser, The mechanism of water oxidation: From electrolysis via homogeneous to biological catalysis, *ChemCatChem* 2(7), 724 (2010)

3. Z. W. Seh, J. Kibsgaard, C. F. Dickens, I. Chorkendorff, J. K. Nørskov, and T. F. Jaramillo, Combining theory and experiment in electrocatalysis: Insights into materials design, *Science* 355(6321), eaad4998 (2017)
4. T. Reier, M. Oezaslan, and P. Strasser, Electrocatalytic oxygen evolution reaction (OER) on Ru, Ir, and Pt catalysts: A comparative study of nanoparticles and bulk materials, *ACS Catal.* 2(8), 1765 (2012)
5. X. Han, X. Ling, D. Yu, D. Xie, L. Li, S. Peng, C. Zhong, N. Zhao, Y. Deng, and W. Hu, Atomically dispersed binary Co-Ni sites in nitrogen-doped hollow carbon nanocubes for reversible oxygen reduction and evolution, *Adv. Mater.* 31(49), 1905622 (2019)
6. S. Sun, Y. Sun, Y. Zhou, S. Xi, X. Ren, B. Huang, H. Liao, L. P. Wang, Y. Du, and Z. J. Xu, Shifting oxygen charge towards octahedral metal: A way to promote water oxidation on cobalt spinel oxides, *Angew. Chem. Int. Ed.* 58(18), 6042 (2019)
7. Y. Duan, Z. Y. Yu, S. J. Hu, X. S. Zheng, C. T. Zhang, H. H. Ding, B. C. Hu, Q. Q. Fu, Z. L. Yu, X. Zheng, J. F. Zhu, M. R. Gao, and S. H. Yu, Scaled-up synthesis of amorphous NiFeMo oxides and their rapid surface reconstruction for superior oxygen evolution catalysis, *Angew. Chem. Int. Ed.* 58(44), 15772 (2019)
8. Y. Shao, X. Xiao, Y. P. Zhu, and T. Y. Ma, Single-crystal cobalt phosphate nanosheets for biomimetic oxygen evolution in neutral electrolytes, *Angew. Chem. Int. Ed.* 58(41), 14599 (2019)
9. R. Chen, S. F. Hung, D. Zhou, J. Gao, C. Yang, H. Tao, H. B. Yang, L. Zhang, L. Zhang, Q. Xiong, H. M. Chen, and B. Liu, Layered structure causes bulk NiFe layered double hydroxide unstable in alkaline oxygen evolution reaction, *Adv. Mater.* 31(41), 1903909 (2019)
10. Y. Zhang, Y. Guo, T. Liu, F. Feng, C. Wang, H. Hu, M. Wu, M. Ni, and Z. Shao, The synergistic effect accelerates the oxygen reduction/evolution reaction in a Zn-Air battery, *Front. Chem.* 7, 524 (2019)
11. Y. Jiao, Y. Zheng, M. Jaroniec, and S. Z. Qiao, Design of electrocatalysts for oxygen- and hydrogen-involving energy conversion reactions, *Chem. Soc. Rev.* 44(8), 2060 (2015)
12. Y. Zheng, Y. Jiao, J. Chen, J. Liu, J. Liang, A. Du, W. Zhang, Z. Zhu, S. C. Smith, M. Jaroniec, G. Q. Lu, and S. Z. Qiao, Nanoporous graphitic-C_3N_4@carbon metal-free electrocatalysts for highly efficient oxygen reduction, *J. Am. Chem. Soc.* 133(50), 20116 (2011)
13. Y. Zheng, Y. Jiao, Y. Zhu, L. H. Li, Y. Han, Y. Chen, A. Du, M. Jaroniec, and S. Z. Qiao, Hydrogen evolution by a metal-free electrocatalyst, *Nat. Commun.* 5(1), 3783 (2014)
14. C. Meng, M. Lin, X. Sun, X. Chen, X. Chen, X. Du, and Y. Zhou, Laser synthesis of oxygen vacancy-modified CoOOH for highly efficient oxygen evolution, *Chem. Commun.* 55(20), 2904 (2019)
15. Z. Zhang, X. Li, C. Zhong, N. Zhao, Y. Deng, X. Han, and W. Hu, Spontaneous synthesis of silver-nanoparticle-decorated transition-metal hydroxides for enhanced oxygen evolution reaction, *Angew. Chem. Int. Ed.* 59(18), 7245 (2020)
16. Y. Xu, F. Zhang, T. Sheng, T. Ye, D. Yi, Y. Yang, S. Liu, X. Wang, and J. Yao, Clarifying the controversial catalytic active sites of Co_3O_4 for the oxygen evolution reaction, *J. Mater. Chem. A* 7(40), 23191 (2019)
17. R. Wei, X. Bu, W. Gao, R A B. Villaos, G. Macam, Z. Q. Huang, C. Lan, F. C. Chuang, Y. Qu, and J. C. Ho, Engineering surface structure of spinel oxides via high-valent vanadium doping for remarkably enhanced electrocatalytic oxygen evolution reaction, *ACS Appl. Mater. Interfaces* 11(36), 33012 (2019)
18. W. Zhang, Y. Wang, H. Zheng, R. Li, Y. Tang, B. Li, C. Zhu, L. You, M. R. Gao, Z. Liu, S. H. Yu, and K. Zhou, Embedding ultrafine metal oxide nanoparticles in monolayered metal–organic framework nanosheets enables efficient electrocatalytic oxygen evolution, *ACS Nano* 14(2), 1971 (2020)
19. L. Wen, X. Zhang, J. Liu, X. Li, C. Xing, X. Lyu, W. Cai, W. Wang, and Y. Li, Cr-dopant induced breaking of scaling relations in CoFe layered double hydroxides for improvement of oxygen evolution reaction, *Small* 15(35), 1902373 (2019)
20. L. J. Enman, A. E. Vise, M. Burke Stevens, and S. W. Boettcher, Effects of metal electrode support on the catalytic activity of Fe(oxy)hydroxide for the oxygen evolution reaction in alkaline media, *ChemPhysChem* 20(22), 3089 (2019)
21. F. Bizzotto, H. Ouhbi, Y. Fu, G. K. H. Wiberg, U. Aschauer, and M. Arenz, Examining the structure sensitivity of the oxygen evolution reaction on Pt single-crystal electrodes: A combined experimental and theoretical study, *ChemPhysChem* 20(22), 3154 (2019)
22. S. Laha, Y. Lee, F. Podjaski, D. Weber, V. Duppel, L. M. Schoop, F. Pielnhofer, C. Scheurer, K. Müller, U. Starke, K. Reuter, and B. V. Lotsch, Ruthenium oxide nanosheets for enhanced oxygen evolution catalysis in acidic medium, *Adv. Energy Mater.* 9(15), 1803795 (2019)
23. S. J. Clark, M. D. Segall, C. J. Pickard, P. J. Hasnip, M. I. J. Probert, K. Refson, and M. C. Payne, First principles methods using CASTEP, *Zeitschrift für Kristallographie - Cryst. Mater.* 220(5–6), 567 (2005)
24. E. R. McNellis, J. Meyer, and K. Reuter, Azobenzene at coinage metal surfaces: Role of dispersive van der Waals interactions, *Phys. Rev. B* 80(20), 205414 (2009)
25. J. P. Perdew, J. A. Chevary, S. H. Vosko, K. A. Jackson, M. R. Pederson, D. J. Singh, and C. Fiolhais, Atoms, molecules, solids, and surfaces: Applications of the generalized gradient approximation for exchange and correlation, *Phys. Rev. B* 46(11), 6671 (1992)
26. P. E. Blöchl, Projector augmented-wave method, *Phys. Rev. B* 50(24), 17953 (1994)
27. H. J. Monkhorst and J. D. Pack, Special points for Brillouin-zone integrations, *Phys Rev B* 13(12), 5188 (1976)
28. S. Grimme, J. Antony, S. Ehrlich, and H. Krieg, A consistent and accurate *abinitio* parametrization of density functional dispersion correction (DFT-D) for the 94 elements H-Pu, *J. Chem. Phys.* 132(15), 154104 (2010)

29. V. D. Mello, L. I. Zawislak, J. B. Marimon da Cunha, E. J. Kinast, J. B. Soares, and C. A. dos Santos, Structure and magnetic properties of layered $(Fe_xCo_{1-x})Ta_2O_6$ compounds, *J. Magn. Magn. Mater.* 196–197, 846 (1999)
30. I. S. Mulla, N. Natarajan, A. B. Gaikwad, V. Samuel, U. N. Guptha, and V. Ravi, A coprecipitation technique to prepare $CoTa_2O_6$ and $CoNb_2O_6$, *Mater. Lett.* 61(11–12), 2127 (2007)
31. J. N. Reimers, J. E. Greedan, C. V. Stager, and R. Kremer, Crystal structure and magnetism in $CoSb_2O_6$ and $CoTa_2O_6$, *J. Solid State Chem.* 83(1), 20 (1989)
32. R. K. Kremer, J. E. Greedan, E. Gmelin, W. Dai, M. A. White, S. M. Eicher, and K. J. Lushington, Specific heat of MTa_2O_6 (M = Co, Ni, Fe, Mg) evidence for low dimensional magnetism, *J. Phys. Colloques* 49(C8), C8-1495 (1988)
33. J. K. Nørskov, J. Rossmeisl, A. Logadottir, L. Lindqvist, J. R. Kitchin, T. Bligaard, and H. Jónsson, Origin of the overpotential for oxygen reduction at a fuel-cell cathode, *J. Phys. Chem. B* 108(46), 17886 (2004)
34. X. Cui, P. Ren, D. Deng, J. Deng, and X. Bao, Single layer graphene encapsulating non-precious metals as high-performance electrocatalysts for water oxidation, *Energy Environ. Sci.* 9(1), 123 (2016)
35. T. Zhang, J. Du, P. Xi, and C. Xu, Hybrids of cobalt/iron phosphides derived from bimetal–organic frameworks as highly efficient electrocatalysts for oxygen evolution reaction, *ACS Appl. Mater. Interfaces* 9(1), 362 (2017)
36. M. Asnavandi, Y. Yin, Y. Li, C. Sun, and C. Zhao, Promoting oxygen evolution reactions through introduction of oxygen vacancies to benchmark NiFe–OOH catalysts, *ACS Energy Lett.* 3(7), 1515 (2018)
37. W. Zhou, D. D. Huang, Y. P. Wu, J. Zhao, T. Wu, J. Zhang, D. S. Li, C. Sun, P. Feng, and X. Bu, Stable hierarchical bimetal–organic nanostructures as high performance electrocatalysts for the oxygen evolution reaction, *Angew. Chem. Int. Ed.* 58(13), 4227 (2019)
38. Y. Wang, Y. Shao, D. W. Matson, J. Li, and Y. Lin, Nitrogen-doped graphene and its application in electrochemical biosensing, *ACS Nano* 4(4), 1790 (2010)
39. Z. Wang, Z. X. Low, X. Zeng, B. Su, Y. Yin, C. Sun, T. Williams, H. Wang, and X. Zhang, Vertically-heterostructured TiO_2–Ag-rGO ternary nanocomposite constructed with 001 facetted TiO_2 nanosheets for enhanced Pt-free hydrogen production, *Int. J. Hydrogen Energy* 43(3), 1508 (2018)
40. T. Liao, Z. Sun, C. Sun, S. X. Dou, and D. J. Searles, Electronic coupling and catalytic effect on H_2 evolution of MoS_2/graphene nanocatalyst, *Sci. Rep.* 4(1), 6256 (2015)
41. B. Fei, Z. Chen, Y. Ha, R. Wang, H. Yang, H. Xu, and R. Wu, Anion-cation Co-substitution activation of spinel $CoMoO_4$ for efficient oxygen evolution reaction, *Chem. Eng. J.* 394, 124926 (2020)
42. M. Hu, S. Li, S. Zheng, X. Liang, J. Zheng, and F. Pan, Tuning single-atom catalysts of nitrogen-coordinated transition metals for optimizing oxygen evolution and reduction reactions, *J. Phys. Chem. C* 124(24), 13168 (2020)
43. J. C. Lei, X. Zhang, and Z. Zhou, Recent advances in MXene: Preparation, properties, and applications, *Front. Phys.* 10(3), 276 (2015)
44. J. Mao, Y. Wang, Z. Zheng, and D. Deng, The rise of two-dimensional MoS_2 for catalysis, *Front. Phys.* 13(4), 138118 (2018)
45. Z. Cui, W. Du, C. Xiao, Q. Li, R. Sa, C. Sun, and Z. Ma, Enhancing hydrogen evolution of MoS_2 Basal planes by combining single-boron catalyst and compressive strain, *Front. Phys.* 15(6), 63502 (2020)